Heterogeneous Catalysis

DOI: 10.1002/anie.201208582

Enhancing Electrocatalytic Oxygen Reduction on MnO_2 with Vacancies**

Fangyi Cheng, Tianran Zhang, Yi Zhang, Jing Du, Xiaopeng Han, and Jun Chen**

Electrochemical oxygen reduction reactions (ORRs) play pivotal roles in various energy storage and conversion technologies, such as metal–air batteries and fuel cells.[1] The sluggish ORR requires catalysts, of which platinum-based materials are known to exhibit the best overall performance.[2] However, the high price and scarcity of platinum necessitates either an increase in the efficiency of noble metal use or the exploitation of non-precious electrocatalysts.[3–7] Among noble-metal-free alternatives, manganese oxides have received intensive attention because of their high element abundance, low cost, lower environmental impact, and moderate activity.[8–16] Manganese oxides can also serve in catalytic oxygen evolution reactions (OERs),[11,16–20] thus making them attractive as bifunctional catalysts for oxygen electrochemistry. Compared with noble-metal catalysts, manganese oxides are generally less active, particularly in terms of overpotentials and their capability to catalyze 4-electron reduction.[7,21] Strategies to enhance the electrocatalytic performance of manganese oxides include doping with cations, coating with metals, and integrating conductive nanostructures.[8,9,21–25] Although these approaches have proven effective, they are relatively complicated and costly. Improving the activity of manganese oxides through simple and economic alternative routes is of great interest for developing high-performing manganese-based electrocatalysts.

Herein, we report a facile strategy for enhancing the activity of MnO_2 by introducing native oxygen defects without modification by foreign additives. Although the importance of oxygen defects in oxides has been demonstrated in different electrochemical systems such as lithium batteries and solid oxide fuel cells,[26–30] to our knowledge little has been reported in the context of ORR under aqueous conditions.[13] Herein, we present the first detailed investigation of the effect of oxygen nonstoichiometry on ORR electrocatalysis in alkaline electrolytes, in conjunction with density functional theory (DFT) calculations and experimental studies. We selected rutile-type β-MnO_2 (Figure 1a) as a model binary manganese oxide because it is a thermodynamically stable phase with obtainable high phase purity.[31]

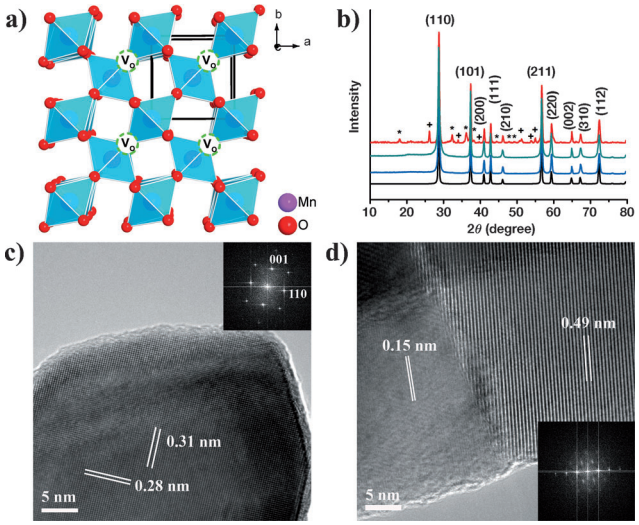

Figure 1. a) Structure of rutile-type MnO_2 with oxygen vacancies. b) XRD patterns of different oxides. The symbols * and + denote Mn_3O_4 and MnOOH, respectively. Pristine (——), H/Ar-350-2h (——), Air-350-2h (——), Ar-350-2h (——), c) and d) HRTEM images of pristine β-MnO_2 (c) and β-MnO_2 heated in Ar (d), the insets show the FFT patterns.

Oxygen deficiencies were introduced into manganese oxides by simple heat treatment. Thermogravimetric (TG) analysis of β-MnO_2 under Ar and air flow shows weight loss at different steps (Supporting Information, Figure S1 and S2), which can be sequentially ascribed to the removal of physisorbed species, the slight release of lattice oxygen, and the phase change from MnO_2 to Mn_2O_3 and Mn_3O_4.[32] The corresponding peak temperatures are higher in air than in Ar. This is reasonable, considering the different oxygen partial pressure between atmospheres of Ar and air. A programmed TG analysis (Figure S3) further indicates that upon heating the oxide loses weight to a larger extent in Ar than in air. Thus, the concentration of oxygen defects is adjustable with the calcination parameters. We prepared a batch of samples by heating MnO_2 under controlled conditions (Figure S4).

Figure 1b shows the powder X-ray diffraction (XRD) patterns of pristine and heat-treated MnO_2 samples. The pattern of pristine MnO_2 is readily indexed to a high-purity pyrolusite phase. The sharp peaks reveal high crystallinity, which is also indicated by the single crystalline character in transmission electron microscopy (TEM) imaging (Figure 1c). The phase purity is maintained on heating the samples below 400 °C in Ar or Air. In comparison, Mn_3O_4 and MnOOH can be detected in the oxide heated in a reducing

[*] Prof. Dr. F. Cheng, T. Zhang, Y. Zhang, J. Du, X. Han, Prof. Dr. J. Chen
Key Laboratory of Advanced Energy Materials Chemistry (Ministry of Eduction), College of Chemistry
Nankai University, Tianjin 300071 (China)
E-mail: fycheng@nankai.edu.cn
chenabc@nankai.edu.cn

[**] This work was supported by the National Programs 973 (2011CB935900) and 863 (2011AA050704), the NSFC (21231005), and the 111 Project (B12015).

Supporting information for this article is available on the WWW under http://dx.doi.org/10.1002/anie.201208582.

atmosphere of Ar/H_2. The structural and compositional information for typical samples is summarized in Table 1. The lattice parameters for a pristine specimen and a specimen annealed in air at 250 °C for 2 h (Air-250-2h; for details on sample naming conventions, see the Experimental Section)

Table 1: Characteristics of pristine and treated β-MnO_2 samples.

Sample[a]	Lattice parameters a/c [Å][b]	Mn valence state[c]	Composition[d]
pristine	4.401/2.875	3.96	$MnO_{1.98}$
Air-250-2h	4.399/2.874	3.98	$MnO_{1.98}$
Air-400-2h	4.406/2.875	3.94	$MnO_{1.97}$
Ar-350-2h	4.408/2.876	3.91	$MnO_{1.96}$
Ar-450-6h	4.412/2.879	3.83	$MnO_{1.92}$

[a] Sample names are given in the format: annealing atmosphere-annealing temperature-annealing time. [b] From XRD Rietveld refinement. [c] From chemical titration. [d] Average data from atomic absorption and emission spectroscopies.

agree well with standard values (JCPDS Card no. 24-0735). For other annealed samples, there is weak lattice expansion, as would be expected from the presence of oxygen vacancies and a larger Mn^{3+} ionic radius. They show the lower average oxidation state of Mn and lower oxygen content, as determined by chemical titration and atomic absorption/emission spectroscopy. Thus, heat treatment in Ar and Air leads to oxygen nonstoichiometry, which is compensated for by the reduction of Mn^{4+} to Mn^{3+}. As the formation of oxygen vacancies is endothermic,[33] an elevated annealing temperature and a prolonged dwell time favor a high concentration of oxygen defects. It should be noted that β-MnO_2 heated to 500 °C displays structural modification. As shown in Figure 1 d, two domains can be observed, which is indicative of a typical pyrolusite lattice and a new structure that corresponds to a different fast Fourier transformation (FFT) pattern. The new lattice fringes and FFT profile can possibly be ascribed to reconstruction and phase transformation, similar to previously reported oxygen-vacancy-induced structural variations of MnO_2.[34]

The ORR activities of pristine and oxygen-vacant β-MnO_2 were investigated using rotational ring-disk electrodes (RRDEs). Figure 2 a shows the typical voltammograms at a potential scanning rate of 5 mV s^{-1}. The disk currents reflect the catalytic ORR, as the cathodic currents are negligible in an Ar-saturated electrolyte (Figure S5). Compared to neat carbon, the oxides are significantly more active in terms of lower overpotentials and larger currents. For the oxides, the oxygen-defective samples exhibit approximately 50 mV higher potential than pristine MnO_2 at a given specific current within the half-wave potential range (Figure 2 b). Accordingly, the introduction of oxygen vacancies enhances the catalytic activity of MnO_2. The ORR kinetics can be also assessed by the Koutecky–Levich (K–L) curves constructed from rotation-speed-dependent current (Figure S5).[13–15] The slopes of the linear plots (Figure 2 c) indicate a dominating 2 e^- ORR process for carbon and a quasi-4 e^- reduction pathway for MnO_2.

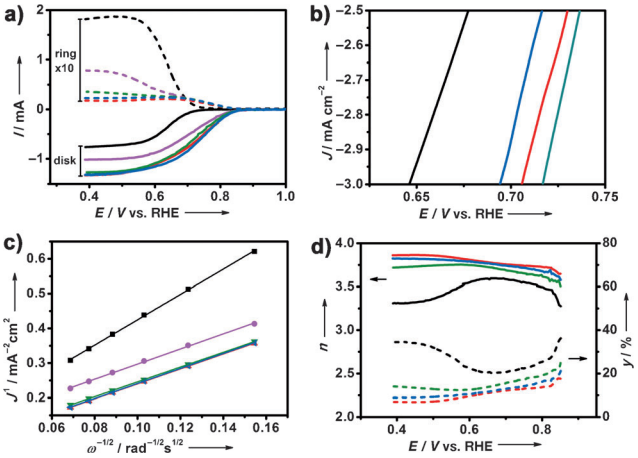

Figure 2. Electrocatalytic properties of pristine and oxygen-vacant β-MnO_2. a) Voltammograms of the ORR using RRDEs in KOH (0.1 M) saturated with O_2. Carbon (——), pristine (——), Ar-350-2h (——), Ar-350-4h (——), Air-400-2h (——). b) Specific activities near the half-wave potential region. pristine (——), Ar-350-2h (——), Ar-350-4h (——), Air-400-2h (——). c) K–L plots at 0.5 V. Carbon (■), pristine (●), Ar-350-2h (▲), Ar-350-4h (▼), Air-400-2h (◀). d) Determined electron transfer number and percentage of peroxide at various potentials. pristine (——), Ar-350-2h (——), Ar-350-4h (——), Air-400-2h (——).

The ORR catalytic performance is further evaluated by calculating the electron transfer number (n) and peroxide yield (y, percentage of HO_2^- relative to total products) from the ring/disk currents (I_R/I_D) through the following equations:

$$n = 4NI_D/(NI_D + I_R) \quad (1)$$

$$y = 200I_R/(NI_D + I_R) \quad (2)$$

where N is the current collection efficiency of RRDE.[8,9,14,35] For oxygen-nonstoichiometric oxides, the obtained electron transfer number is above 3.7 over the potential range of 0.40–0.65 V. This suggests an apparent 4 e^- reduction, which is consistent with the results from the K–L determination. The lower n and higher y on pristine MnO_2 again indicates the enhancement of the ORR by oxygen deficiency. Interestingly, the Air-400-2h and Ar-350-2h samples outperform the Ar-350-4h sample to some extent. The heat treatment parameters affect the ORR activity (Figure S6); the optimized annealing temperature and time were found to be 350–400 °C and ca. 2 h, respectively. Thus, the most efficient MnO_2 catalyst features a modest concentration of oxygen vacancies. Compared with conventional methods (such as Ni doping) for modifying MnO_2,[36] the present facile thermal treatment strategy renders more prominent improvement in currents, potentials, and electrons transferred.

Besides improved activity, the oxygen-vacant oxide exhibits slightly better catalytic durability than pristine oxide in a continuous polarization over 24 h (Figure S7). Additionally, the shape and slopes of the Tafel curves are close for all MnO_2 catalysts (Figure S8), which indicates similar ORR reaction mechanisms. Furthermore, preliminary results show that, compared to the pristine oxide, oxygen-

defective MnO_2 exhibits better activity for OERs (Figure S9). In the context of ORR–OER bifunctional catalysts, which play important role in rechargeable metal–air batteries,[6,7] favoring OER is an additional merit of oxygen nonstoichiometry.

To understand the positive attribute of oxygen vacancies, we have performed DFT modeling, which is a useful tool for elucidatinge the likely reaction mechanism in the ORR catalytic cycle.[37,38] We focused on the ORR on the stable and preferentially exposed MnO_2 (110) surface (Figure S10). In alkaline media, the ORR involves complex processes associated with several oxygen-containing species.[1] We first considered the interaction between the catalyst surface and O_2/H_2O. The calculation indicates that H_2O is preferentially absorbed over O_2 on the 5 fold-coordinated surface Mn ions (Mn_{5c}; Figure S11). Moreover, the surface with full H_2O coverage is the most thermodynamically stable. The splitting of adsorbed H_2O forms a hydroxylated surface, which appears to be the initial state for the ORR. Accordingly, three models were constructed for MnO_2: the perfect surface and the surfaces with one and two oxygen vacancies (Figure 3a). These optimized structures clearly reveal that the introduction of vacancies modifies the Mn–O bond and the surface configuration.

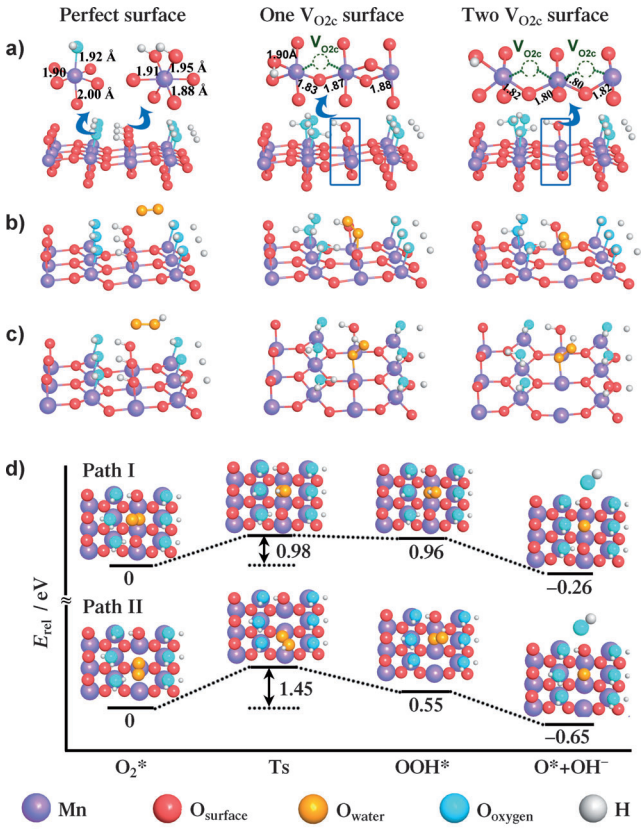

Figure 3. a) Constructed models of perfect and oxygen-vacant hydroxylated β-MnO_2 (110) surfaces. b) and c) Configurations of O_2 (b) and OOH (c) adsorbed on different surfaces. d) Energy profiles and configurations of ORR on β-MnO_2 surfaces with one (Path I) and two (Path II) oxygen vacancies. Asterisks denote adsorbed species. TS = transition state.

We next modeled the adsorption of oxygen and peroxide on different hydroxylated MnO_2 surfaces (Figure 3b,c). For a perfect surface, O_2 is very weakly bound, with an adsorption energy of only 0.07 eV. In comparison, the binding of O_2 to one and two O_{2c} vacant surfaces is observed in the bridge form (two O atoms on two Mn atoms) and in the Griffith form (two O atoms on one Mn atom), respectively. After adsorption onto oxygen-defect surfaces, the O–O bond is elongated (1.26 and 1.34 Å vs. 1.24 Å before adsorption), which indicates an activation and partial dissociation of O_2. The adsorption energies for one-vacancy and two-vacancy surfaces are 0.13 and 0.33 eV, which is about 2- and 5-fold higher, respectively, than that of a perfect surface. Such enhanced binding of O_2 is further verified by overlapping of the Mn 3d orbital and O 2p orbital in the projected density of states (PDOS) profiles (Figure S12). Similarly, the adsorption of peroxide on oxygen vacant surface is much stronger than that on a perfect surface (Figure 3c). Therefore, the presence of oxygen vacancies enhances the interaction between oxygen-containing species and MnO_2 surfaces.

On metal-oxide catalyst surfaces, the ORR in alkaline media is proposed to proceed through steps including hydroxide displacement, peroxide and oxide formation, and hydroxide regeneration.[1,7,9,13] The reduction of adsorbed O_2 to adsorbed peroxide is likely the rate determining step. Thus, the energy profiles of this process were calculated (Figure 3d). For the perfect β-MnO_2 (110) surface, the formation of OOH* is endothermic by 3.09 eV (Figure S13), which implies that the process is thermodynamically unfavorable. This energy decreases to 0.96 and 0.55 eV by introducing one and two O_{2c} vacancies, respectively. As a result, oxygen deficiency benefits the ORR on β-MnO_2 with regards to thermodynamics; higher vacancy content exerts a more positive effect. Note that the peroxides formed can easily decompose through an exothermic reduction process, making the overall ORR thermodynamically feasible. Remarkably, the one-oxygen-vacant surface affords a much lower energy barrier than the two-oxygen-vacant surface does (0.98 vs. 1.45 eV), which is suggestive of improved kinetics. As the major drawback for ORR is the sluggish kinetics, the one-oxygen-vacant oxide should result in higher catalytic activity. This is consistent with electrochemical results (Figure 2). Furthermore, the oxygen vacancy content in the calculated β-MnO_2 supercell is 1.4 atom%, which is close to the measured values of the most active Air-400-2h and Ar-350-2h oxide samples. Therefore, both computational and experimental investigations suggest that a modest oxygen vacancy is desirable for MnO_2-based catalysts.

In conclusion, we have shown that the catalytic activity of MnO_2 for the ORR can be enhanced without introducing foreign components by generating an oxygen deficiency. Oxides with an adjustable concentration of oxygen vacancies have been prepared by simply heating MnO_2 in Ar or Air. The oxygen-vacancy-bearing oxide enables more positive potential, larger current, and lower peroxide yield for the ORR electrocatalysis process, and also favors OER catalysis. DFT computational studies reveal contributions from modified surface–oxygen interaction and a reduced kinetic barrier. This finding could widen the application potential of cheap,

abundant, and bifunctional Mn-based oxide catalysts and provide insight into the importance of oxygen nonstoichiometry in oxygen electrochemistry.

Experimental Section

Pristine β-MnO_2 nanorods were prepared by a hydrothermal route.[23] The resulting nanorods were kept at desired temperatures in a flowing gas stream to synthesize different oxygen-vacant MnO_2 samples. The obtained specimens are denoted in the format: annealing atmosphere-annealing temperature-annealing time. For example, Ar-350-2h denotes a sample prepared by heating pristine nanorods at 350 °C for 2 h in Ar. For electrochemical tests, a three-electrode cell was used with a saturated calomel reference electrode (SCE), a Pt counter electrode, and a catalyst-coated working electrode. Potentials were referenced to the reversible hydrogen electrode (RHE) potential scale. Computational studies were carried out using a periodic plane-wave DFT method. Details on preparation, characterization, and calculations can be found in the Supporting Information.

Received: October 25, 2012
Published online: January 25, 2013

Keywords: density functional theory · electrochemistry · manganese oxide · oxygen reduction · vacancy

[1] K. Kinoshita, *Electrochemical Oxygen Technology*, Wiley, New York, **1992**.
[2] H. A. Gasteiger, S. S. Kocha, B. Sompalli, F. T. Wagner, *Appl. Catal. B* **2005**, *56*, 9.
[3] A. Kloke, F. von Stetten, R. Zengerle, S. Kerzenmacher, *Adv. Mater.* **2011**, *23*, 4976.
[4] Y. J. Feng, N. Alonso-Vante, *Phys. Status Solidi B* **2008**, *245*, 1792.
[5] Z. W. Chen, D. Higgins, A. Yu, L. Zhang, J. J. Zhang, *Energy Environ. Sci.* **2011**, *4*, 3167.
[6] R. Cao, J. S. Lee, M. Liu, J. Cho, *Adv. Energy Mater.* **2012**, *2*, 816.
[7] F. Cheng, J. Chen, *Chem. Soc. Rev.* **2012**, *41*, 2172.
[8] M. S. El-Deab, T. Ohsaka, *Angew. Chem.* **2006**, *118*, 6109; *Angew. Chem. Int. Ed.* **2006**, *45*, 5963.
[9] I. Roche, E. Chaînet, M. Chatenet, J. Vondrák, *J. Phys. Chem. C* **2007**, *111*, 1434.
[10] A. Débart, A. J. Paterson, J. Bao, P. G. Bruce, *Angew. Chem.* **2008**, *120*, 4597; *Angew. Chem. Int. Ed.* **2008**, *47*, 4521.
[11] Y. Gorlin, T. F. Jaramillo, *J. Am. Chem. Soc.* **2010**, *132*, 13612.
[12] L. Jin, L. Xu, C. Morein, C. Chen, M. Lai, S. Dharmarathna, A. Dobley, S. L. Suib, *Adv. Funct. Mater.* **2010**, *20*, 3373.
[13] J. Suntivich, H. A. Gasteiger, N. Yabuuchi, H. Nakanishi, J. B. Goodenough, Y. Shao-Horn, *Nat. Chem.* **2011**, *3*, 546.
[14] Y. Liang, H. Wang, J. Zhou, Y. Li, J. Wang, T. Regier, H. J. Dai, *J. Am. Chem. Soc.* **2012**, *134*, 3517.
[15] F. Cheng, J. Shen, B. Peng, Y. Pan, Z. Tao, J. Chen, *Nat. Chem.* **2011**, *3*, 79.
[16] K. L. Pickrahn, S. W. Park, Y. Gorlin, H. Lee, T. F. Jaramillo, S. F. Bent, *Adv. Energy Mater.* **2012**, *2*, 1269.
[17] F. Jiao, H. Frei, *Chem. Commun.* **2010**, *46*, 2920.
[18] D. M. Robinson, Y. B. Go, M. Greenblatt, G. C. Dismukes, *J. Am. Chem. Soc.* **2010**, *132*, 11467.
[19] M. M. Najafpour, T. Ehrenberg, M. Wiechen, P. Kurz, *Angew. Chem.* **2010**, *122*, 2281; *Angew. Chem. Int. Ed.* **2010**, *49*, 2233.
[20] K. Mette, A. Bergmann, J. P. Tessonnier, M. Hävecker, L. Yao, T. Ressler, R. Schlögl, P. Strasser, M. Behrens, *ChemCatChem* **2012**, *4*, 851.
[21] F. Cheng, Y. Su, J. Liang, Z. Tao, J. Chen, *Chem. Mater.* **2010**, *22*, 898.
[22] M. S. El-Deab, T. Ohsaka, *Electrochim. Acta* **2007**, *52*, 2166.
[23] W. Sun, A. Hsu, R. R. Chen, *J. Power Sources* **2011**, *196*, 4491.
[24] Z. Chen, A. Yu, R. Ahmed, H. J. Wang, H. Li, Z. W. Chen, *Electrochim. Acta* **2012**, *69*, 295.
[25] T. N. Lambert, D. J. Davis, W. Lu, S. J. Limmer, P. G. Kotula, A. Thuli, M. Hungate, G. Ruan, Z. Jin, J. M. Tour, *Chem. Commun.* **2012**, *48*, 7931.
[26] J. Y. Shin, J. H. Joo, D. Samuelis, J. Maier, *Chem. Mater.* **2012**, *24*, 543.
[27] H. Ullmann, N. Trofimenko, F. Tietz, D. Stöver, A. Ahmad-Khanlou, *Solid State Ionics* **2000**, *138*, 79.
[28] R. Merkle, J. Maier, *Angew. Chem.* **2008**, *120*, 3936; *Angew. Chem. Int. Ed.* **2008**, *47*, 3874.
[29] G. J. la O', S. J. Ahn, E. Crumlin, Y. Orikasa, M. D. Biegalski, H. M. Christen, Y. Shao-Horn, *Angew. Chem.* **2010**, *122*, 5472; *Angew. Chem. Int. Ed.* **2010**, *49*, 5344.
[30] S. H. Oh, L. F. Nazar, *Adv. Energy Mater.* **2012**, *2*, 903.
[31] Y. Chabre, J. Pannetier, *Prog. Solid State Chem.* **1995**, *23*, 1.
[32] R. Giovanoli, *Thermochim. Acta* **1994**, *234*, 303.
[33] C. Sun, Y. Wang, J. Zou, S. C. Smith, *Phys. Chem. Chem. Phys.* **2011**, *13*, 11325.
[34] Y. Wang, C. Sun, J. Zou, L. Wang, S. Smith, G. Q. Lu, D. J. H. Cockayne, *Phys. Rev. B* **2010**, *81*, 081401.
[35] X. Han, T. Zhang, J. Du, F. Cheng, J. Chen, *Chem. Sci.* **2013**, *4*, 368.
[36] A. C. Garcia, A. D. Herrera, E. A. Ticianelli, M. Chatenet, C. Poinsignon, *J. Electrochem. Soc.* **2011**, *158*, B290.
[37] Y. Choi, M. C. Lin, M. Liu, *Angew. Chem.* **2007**, *119*, 7352; *Angew. Chem. Int. Ed.* **2007**, *46*, 7214.
[38] H. Y. Su, Y. Gorlin, I. C. Man, F. Calle-Vallejo, J. K. Nørskov, T. F. Jaramillo, J. Rossmeisl, *Phys. Chem. Chem. Phys.* **2012**, *14*, 14010.

